



**HAL**  
open science

# Ultrafast Photoinduced Dynamics of 1,3-Cyclohexadiene Using XMS-CASPT2 Surface Hopping

Iakov Polyak, Lewis Hutton, Rachel Crespo-Otero, Mario Barbatti, Peter Knowles

► **To cite this version:**

Iakov Polyak, Lewis Hutton, Rachel Crespo-Otero, Mario Barbatti, Peter Knowles. Ultrafast Photoinduced Dynamics of 1,3-Cyclohexadiene Using XMS-CASPT2 Surface Hopping. *Journal of Chemical Theory and Computation*, 2019, 15 (7), pp.3929-3940. 10.1021/acs.jctc.9b00396 . hal-02288616

**HAL Id: hal-02288616**

**<https://amu.hal.science/hal-02288616>**

Submitted on 15 Sep 2019

**HAL** is a multi-disciplinary open access archive for the deposit and dissemination of scientific research documents, whether they are published or not. The documents may come from teaching and research institutions in France or abroad, or from public or private research centers.

L'archive ouverte pluridisciplinaire **HAL**, est destinée au dépôt et à la diffusion de documents scientifiques de niveau recherche, publiés ou non, émanant des établissements d'enseignement et de recherche français ou étrangers, des laboratoires publics ou privés.

# Ultrafast photo-induced dynamics of 1,3-cyclohexadiene using XMS-CASPT2 surface hopping

Iakov Polyak,<sup>\*,†</sup> Lewis Hutton,<sup>†</sup> Rachel Crespo-Otero,<sup>‡</sup> Mario Barbatti,<sup>¶</sup> and  
Peter J. Knowles<sup>\*,†</sup>

<sup>†</sup>*School of Chemistry, Cardiff University, Cardiff CF10 3AT, United Kingdom*

<sup>‡</sup>*School of Biological and Chemical Sciences, Queen Mary University of London, Mile End  
Road, London E1 4NS, United Kingdom*

<sup>¶</sup>*Aix-Marseille Univ, CNRS, ICR, Marseille, France*

E-mail: PolyakI@Cardiff.ac.uk; KnowlesPJ@Cardiff.ac.uk

## Abstract

A full-dimensional simulation of the photo-dissociation of 1,3-cyclohexadiene in the manifold of three electronic states was performed via non-adiabatic surface hopping dynamics using extended multi-state complete active space second-order perturbation (XMS-CASPT2) electronic structure theory with fully analytic non-adiabatic couplings. With the  $47 \pm 8\%$  product quantum yield calculated from the 136 trajectories, generally 400 fs-long, and an estimated excited lifetime of  $89 \pm 9$  fs, our calculations provide a detailed description of the non-adiabatic deactivation mechanism, showing the existence of an extended conical intersection seam along the reaction coordinate. The nature of the preferred reaction pathways on the ground state is discussed and extensive comparison to the previously published full dimensional dynamics calculations is provided.

# 1 Introduction

Photo-induced ring opening in cyclohexa-1,3-diene (CHD) (see Fig. 1) is one of the most popular non-adiabatic molecular reactive processes, acting as a prototype for many other photo-induced reactions in larger systems including those of biological importance.<sup>1</sup> Having served as an example of a pericyclic reaction used to explain the Woodward-Hoffman rules,<sup>2</sup> later reformulated by van der Lugt and Oosterhoff for general photoinduced concerted processes,<sup>3</sup> this reaction has been widely studied both experimentally and theoretically. One can conveniently separate the research undertaken into the period covered in the two extensive reviews published in 2011<sup>4</sup> and 2014<sup>1</sup> and the work done since. A rather detailed understanding of the reaction mechanism has been obtained in a series of multielectron dissociative ionization and time-resolved photoelectron spectroscopic studies.<sup>5-11</sup> Experimental findings have been supported by theoretical calculations, including study of potential energy surface (PES) critical points,<sup>7,12-19</sup> restricted-dimensional quantum dynamical,<sup>20-23</sup> and full-dimensional mixed quantum-classical trajectory-based simulations.<sup>24-30</sup> Until recently, the explicit evolution of geometry following photoexcitation could be obtained only from potential surfaces derived from electronic structure calculations; recent advances in ultrafast X-ray sources with high intensity and electron diffraction techniques have allowed for the first direct insights into the sub-picosecond imaging of CHD photodissociation.<sup>31-33</sup> The first X-ray spectroscopic study to directly reveal the valence electronic structure of the transient pericyclic minimum predicted by Lugt and Oosterhoff has also been performed.<sup>34</sup>

The general, however not yet full agreed, view on the reaction mechanism is as follows (see Fig. 1). Excitation (in a conventional, one-photon set-up) from the ground state occurs to the lowest  $\pi\pi^*$ -state (conventionally labeled as  $1^1B$  due to satisfying the  $B$ -symmetry of the  $C_2$  group in the Franck-Condon (FC) region). Dynamics then rapidly proceeds along a narrow channel with the molecule keeping its symmetry while undergoing first the partial double bond pattern reordering (butadiene-like  $\rightarrow$  hexatriene-like) within the closed ring and then the initial ring-opening moiety. The wavepacket then hits the first conical intersection

(CoIn) with the  $2^1A$  state (being itself dark to a one-photon absorption). Having changed the state character and split into the two broken-symmetry parts, the wavepacket proceeds along the flatter reaction path region in the general direction of the two flat  $2^1A$  asymmetric minima.<sup>4,7,9</sup> Somewhere along that path, in the vicinity of the minima, the wavepacket is expected to eventually hit the crossing seam with the ground state, and either return to the reactant minimum, thereby conserving the closed ring structure, or decay into the hexatriene (HT) product, followed by further chain rearrangements between the three possible conformers (cZc-, cZt- and tZt-HT). This seam has been theoretically predicted to have an extended nature, “following along” the wavepacket path on  $2^1A$ .<sup>19</sup> Thus, the photodissociation mechanism involves three diabatic states ( $1^1B$ ,  $2^1A$  and  $1^1A$ ) but the wavepacket is thought to mainly stay on the two adiabatic states ( $S_1$  and  $S_0$ ). This picture has been somewhat questioned and re-considered recently, suggesting that only a single excited state may be involved in the reaction path;<sup>28</sup> however, this model is mainly backed by single-reference linear response time-dependent density functional theory (LR-TD-DFT) calculations, which should be used with extra care in such elaborate non-adiabatic cases like CHD photo-dissociation. It also seems to contradict the results obtained with multi-reference CASPT2 and MRCI calculations.<sup>16–18</sup> Apart from the conventional one-photon-driven process, the recent time-resolved photoelectron and high harmonic spectroscopic studies used a two-photon initial excitation to one of the lowest Rydberg states, followed by longer-time decay dynamics, suggesting the existence of alternative pathway(s) yet to be explained.<sup>35,36</sup>

Following a one-photon absorption at a wavelength around 260 – 270 nm, the  $S_1$  state depopulation time constant estimation has been highly consistent across different experiments, usually amounting to 130 – 140 fs (commonly subdivided into the  $1^1B$  and  $2^1A$  lifetimes, each of which is more broadly estimated to last 30 – 70 fs and 60 – 80 fs correspondingly).<sup>5–11</sup> The time for product formation is also estimated rather broadly in the range 142 – 230 fs.<sup>6,10,11,34</sup>

Photodissociation branching ratio of reactive *vs.* unreactive channels has been a matter of debate, as while in early experiments in solution the quantum yield (QY) has been

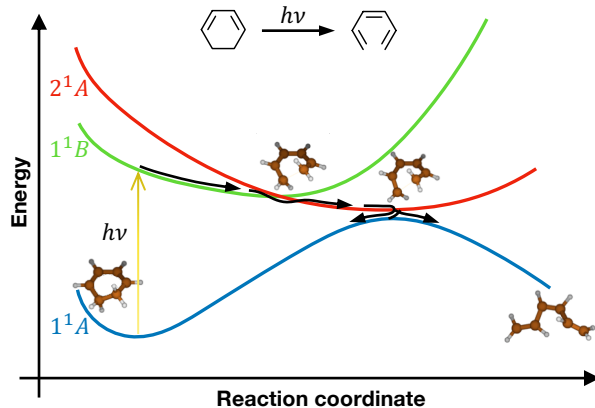


Figure 1: Schematic potential energy curves and reaction pathway for the CHD photodissociation. Chemical structures for the reactant and product are given at the top.

quantitatively estimated to be 41% HT,<sup>37</sup> initial transient electron diffraction studies in the gas phase suggested a 100% product conversion.<sup>38,39</sup> Such a large QY, which however could have been affected by a rather poor time resolution of early diffraction experiments, was in striking contrast to the results of electronic structure calculations, which rather consistently predicted a yield similar to the one shown for the reaction in solution.<sup>14,21–23,25–30</sup> Two later experiments provided an indirect evidence of a non-unit QY in the gas phase (50%<sup>40</sup> and an upper bound of 73%<sup>41</sup>) and finally Adachi *et al.* estimated it as low as 30% by fitting the observed differential photoelectron spectra (averaged over the time range of 510 – 990 fs after initial excitation) into the estimated ones based on He(I) photoelectron spectra.<sup>11</sup>

The nature of the observed branching ratio is not clear either and has been attributed to the local PES topology around the  $S_1/S_0$  CoIn and its location on a hypersurface,<sup>14,22</sup> extended crossing seam,<sup>19</sup> sufficient wavepacket momentum,<sup>26</sup> gained along the stretching carbon-carbon bond<sup>30,42</sup> or more generally along the bond-alternating coordinate.<sup>28</sup>

Theoretical studies of the CHD photodissociation reaction path and dynamics are complicated by the sensitivity of the excited state energies on the electronic structure method and level. Specifically, the order of the  $1^1B$  and  $2^1A$  states in the FC region gets swapped when the widely used state-averaged complete active space self-consistent field method with 6 ac-

tive electrons in 4  $\pi, \pi^*$ - and 2  $\sigma, \sigma^*$ -orbitals (SA-CAS(6,6)SCF) is used. While the ordering improves further down the reaction path (approximately after the  $S_1/S_2$  CoIn), this obviously makes the full-path calculations using the same CASSCF ansatz invalid, forcing some studies to be limited to the part of the reaction happening on  $2^1A$  and  $1^1A$  states only.<sup>12,19–21,23</sup> Significantly increasing the size of (restricted) active space in a consistent manner has been shown to allow for a qualitatively correct state ordering for the butadiene-like molecules.<sup>43</sup> However, quantitatively correct state energies are harder to obtain, while RASSCF with very large active space can be expected to be rather expensive and hard to deal with in dynamics calculations. Martínez *et al.* and Lei *et al.* used clipped active spaces that included only a single ( $\pi^*$ -) virtual orbital (CAS(6,4)<sup>26,44,45</sup> and CAS(14,8)<sup>29</sup> correspondingly), which, while giving the qualitatively right order of states in the FC region, probably reach this effect through error compensation, and are thus rather dangerous to be used in full dimensional on-the-fly dynamic calculations, where far-lying regions of the configuration space may be sampled. Several reaction path studies evaluated potential energy with (MS-)CASPT2 or MRCI (multi-reference configuration interaction) methods at the CASSCF-optimized geometries,<sup>7,13–15,17</sup> with Tamura *et al.* having subsequently performed restricted-dimensional quantum dynamics calculations on the MRCI-fitted PES, using, however, approximate diabatic couplings.<sup>22</sup> Mori and Kato later employed CASPT2 analytic gradient technique to optimize minima and minimum-energy conical intersections (MECI) and emphasized the importance of dynamic electron correlation for obtaining accurate geometries.<sup>18</sup> Recently, Ohta *et al.* performed a full-dimensional surface-hopping dynamics study employing MS-MR-CASPT2 energies and gradients, but using the semi-classical Zhu-Nakamura formula to calculate the non-adiabatic transition probabilities from the SA-CASSCF non-adiabatic couplings (NAC).<sup>27</sup> Non-adiabatic DFT surface-hopping calculations have been also performed, either based on LR-TD-DFT,<sup>25,28</sup> or using state-interaction, state-averaged spin-restricted ensemble-referenced Kohn-Sham (SSR) method.<sup>30</sup> In both cases, however, dynamics have been run on the  $S_1$  and  $S_0$  electronic states only.

All the previous dynamic studies are prone to deficiencies of different types, either connected to the description of the non-adiabatic interaction or of the electronic density. In particular, none of the *ab initio* studies treated all aspects of electronic structure calculations in a balanced way with a consistent level of dynamic correlation, with some relying on CASSCF gradients and others on CASSCF NACs. Recent derivation of the analytic gradients and NAC for XMS-CASPT2,<sup>46,47</sup> and their implementation in the BAGEL electronic-structure program,<sup>48,49</sup> finally made such calculations possible.

We hereby report a full-dimensional non-adiabatic surface-hopping dynamics study of the CHD photodissociation in the manifold of the 3 lowest electronic states of CHD ( $1^1B$ ,  $2^1A$  and  $1^1A$ ) at the XMS-CASPT2 level with the full NACs used to evaluate the transition probabilities on-the-fly. We further note that while most of the previous trajectory-based calculations derived initial conditions from either sampling the ground state Boltzmann ensemble at 300 K,<sup>28,29</sup> or the full-width zero-point energy nuclear wavepacket modeled by a harmonic-oscillator Wigner distribution,<sup>27,30</sup> we herein perform sampling from the narrow excitation frequency domain only, trying to mimic conditions created in experiment due to a finite pump laser half-width as close as we can. A similar approach has been recently employed in an *ab initio* multiple spawning (AIMS) study, performed in support of an electron diffraction experiment.<sup>33</sup>

## 2 Computational details

All electronic structure calculations in the current work have been performed with BAGEL,<sup>48,49</sup> using the XMS-CASPT2 method based on molecular orbitals obtained from the SA-CAS(6,6)SCF for the 3 lowest electronic singlet states. The active space, as depicted in Fig. 2, contained the two (HOMO and HOMO-1)  $\pi$ -orbitals and their anti-bonding  $\pi^*$ -counterparts (LUMO and LUMO+1), as well as the  $\sigma$  and  $\sigma^*$  orbitals initially localized at the bond subject to dissociation ( $C_1 - C_6$ , see Fig. 3 for atom labeling). The level shift parameter of  $0.5 E_h$  has

been added to the zeroth order Hamiltonian in order to circumvent intruder state problems (combined with a level shift correction that removes the effect on the second-order energy)<sup>50</sup> both in reaction path and surface hopping dynamics calculations. In all our calculations, we employed the cc-pVDZ basis set.<sup>51</sup>

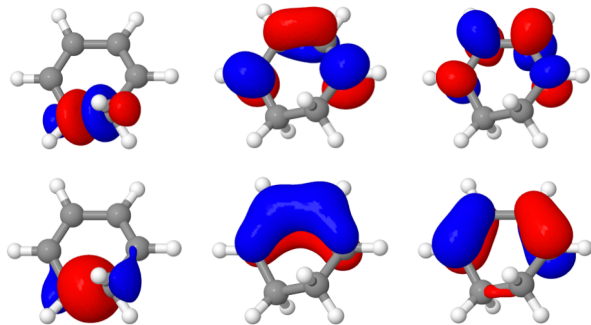


Figure 2: Orbitals constituting active space for SA-CASSCF and XMS-CASPT2 calculations in the current work, given at the equilibrium CHD geometry.

Both the XMS-CASPT2 analytic gradients and NACs are implemented in BAGEL<sup>46,47</sup> and have been used in the current work for the minimum-energy CoIn (MECI) optimizations and surface hopping dynamics calculations. Harmonic frequencies and normal modes for the ground state equilibrium geometry have been calculated numerically by central gradient differences.  $C_2$  symmetry has not been enforced in any of our calculations.

To optimize the MECIs we employed the gradient projection algorithm,<sup>52</sup> as implemented in BAGEL. Optimization runs have been performed in Cartesian coordinates, with the use of the interstate NACs without weighting them by energy gap.

The Newton-X program<sup>53,54</sup> has been used to calculate the absorption cross section spectrum in the FC region and run the surface hopping dynamics calculations. To use the XMS-CASPT2 energies, gradients, frequencies and NACs obtained on-the-fly, we have modified a corresponding interface to BAGEL in the developmental version of Newton-X, originally written by Park and Shiozaki.<sup>46</sup>

To calculate the absorption spectrum and prepare initial conditions for the surface hopping dynamics, the nuclear ensemble approximation was used.<sup>55</sup> 2000 ground-state geome-

tries and velocities have been sampled from a harmonic-oscillator Wigner distribution,<sup>55</sup> using the harmonic CASPT2 frequencies and normal modes obtained at the CHD equilibrium geometry optimized at the same level of theory. The three lowest electronic singlet states ( $1^1B$ ,  $2^1A$  and  $1^1A$ ) have been included in each single point XMS-CASPT2 calculation and used to compute the spectrum. The width of the Lorentzian line shapes was set to 0.05 eV.

Non-adiabatic dynamics calculations have been performed in the manifold of the 3 lowest electronic singlet states after an  $S_0 \rightarrow S_1$  ( $1^1A \rightarrow 1^1B$ ) transition with the decoherence-corrected<sup>56</sup> fewest switches surface hopping<sup>57</sup> (DC-FSSH) method employed to account for the the individual trajectories discretely changing their population (hopping between the adiabatic electronic states). The parameter for the decoherence corrections was set to  $\alpha = 0.1 E_h$ . Analogously to Kosma *et al.*, who pumped CHD with a 12 fs pulse centered at  $37000 \text{ cm}^{-1}$  (4.59 eV) with half-width of  $\sim 2100 \text{ cm}^{-1}$  (0.26 eV),<sup>9</sup> we selected our initial conditions from a 0.2 eV square energy window centered at 4.6 eV. With 2000 geometries sampled overall, 136 of them were in this window and were all used in surface-hopping calculations, together with the associated sampled velocities. The initial adiabatic electronic state population for each trajectory was determined based on the corresponding dipole transition probability, and this resulted in all trajectories starting on  $S_1$  ( $1^1B$ ). The maximum simulation time was 400 fs. The classical equations-of-motion have been integrated with steps of 0.5 fs (or 0.25 fs for those trajectories that failed to conserve the total energy to within 0.5 eV window before decaying to  $S_0$ ; see below), while the time-dependent electronic equations have been propagated with steps of 0.025 fs by using interpolated quantities between the classical steps.

### 3 Results

Fig. 3 depicts the equilibrium (CHD) and the two MECI geometries, optimized with XMS-CASPT2, and defines the atom numbering scheme. Both vertical excitation energies at the FC point (see Table 1) agree within 0.2 eV with those obtained by Mori and Kato,<sup>18</sup> as well as experimental results.<sup>16</sup> The  $2^1A$  excitation energy also agrees within 0.1 eV with the CASPT2 results by Merchán *et al.*,<sup>16</sup> while the  $1^1B$  energy is higher in our calculations by 0.41 eV (but only by 0.19 eV with respect to the experimental value reported in the same work). We note that there is discrepancy with regards to the identity of the second valence excited state energy in the literature. While Merchán *et al.* labeled it as  $4^1A$  (having reserved the labels  $2^1A$  for the  $12a \rightarrow 3s$  and  $3^1A$  for the  $12a \rightarrow 3p_z$  Rydberg states correspondingly),<sup>16</sup> it later became conventional to use the  $2^1A$  label. This has led several authors to use the wrong value when referring to the second valence excited state benchmark energy,<sup>10,35</sup> although those works do not appear to make an extensive use of it. Apart from the equilibrium geometry, both the relative ground and excited state energies, as well as the geometries of the two optimized MECIs ( $S_2/S_1$  and  $S_1/S_0$  correspondingly) are also similar to those obtained by Mori and Kato,<sup>18</sup> however both the breaking bond length ( $r(C_1 - C_6)$ ) at the  $S_2/S_1$  MECI and the larger dihedral angle ( $\angle C_1C_2C_3C_4$ ) at the asymmetric  $S_1/S_0$  MECI are somewhat bigger in our case.

The calculated absorption spectrum arising from the two lowest singlet electronic transitions ( $1^1A \rightarrow 1^1B$  and  $1^1A \rightarrow 2^1A$ ), where only the first transition is bright, overlaps very well with the experimental UV spectrum obtained by Kosma *et al.*<sup>9</sup> (see Fig. 4). Interestingly, the simulated spectrum looks even closer to the transformed spectrum with enhanced vibrational structure, calculated in the same work.<sup>9</sup>

Being interested in the first part of the reaction, up to the point where the wavepacket has fully decayed onto the ground electronic state and split into the two channels that define the reaction QY, we have initially run all trajectories for 200 fs with a step size of 0.5 fs, assuming it would be a long enough simulation for all trajectories to decay to  $S_0$ , according

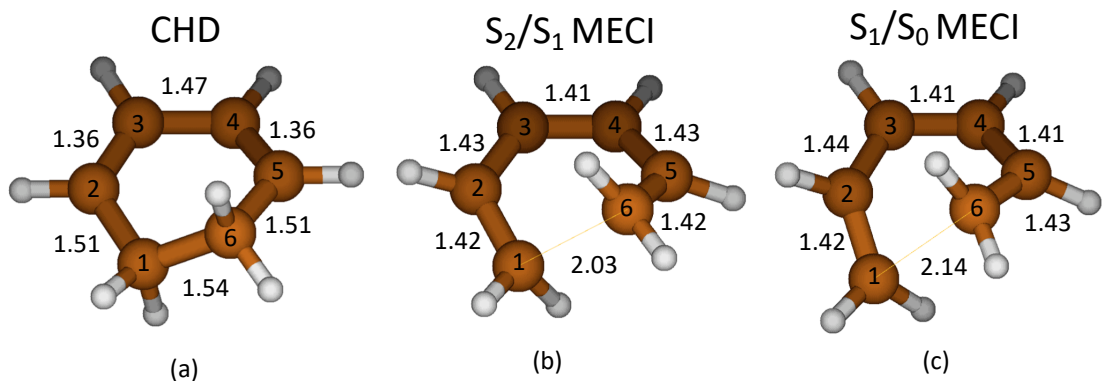


Figure 3: Equilibrium and the two MECI geometries optimized with XMS-CASPT2, with the carbon atom numbers given as used in this work. Distances are in Å.

Table 1: Energies of the lowest three singlet states and characteristic internal coordinates at the equilibrium and MECI geometries, calculated with XMS-CASPT2. Energies are in eV, distances are in Å and angles are in degrees. The ground state energy of CHD was set to zero.

	CHD	S <sub>2</sub> /S <sub>1</sub> MECI	S <sub>1</sub> /S <sub>0</sub> MECI
Internal coordinates			
$r(C_1 - C_6)$	1.54	2.03	2.14
$\angle C_1 C_2 C_3 C_4$	-2.16	-16.55	-31.82
$\angle C_6 C_5 C_4 C_3$	-2.15	-16.60	-9.88
Energy			
$1^1A$	0.00	2.66	3.80
$1^1B$	5.13	4.39	6.28
$2^1A$	6.28	4.39	3.80

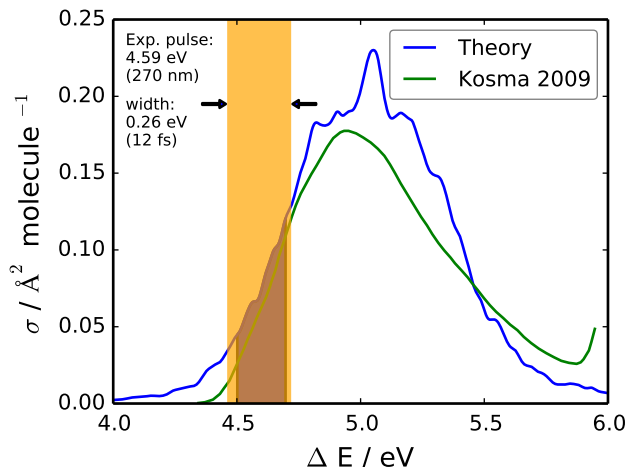


Figure 4: Absorption cross section spectrum calculated in the current work, overlapped with the experimentally obtained UV spectrum by Kosma *et al.*<sup>9</sup> The pump pulse temporal and frequency width is indicated (orange bar), as well as the range of transition energies, from within which the initial conditions for surface-hopping calculations have been taken (filled area under the calculated spectrum).

to most of the previous findings. Out of 136 trajectories, 18 failed to conserve the total energy within the defined threshold (we note that the orbitals in the active space for such trajectories retained their identity, however the cause for the failures still lies in the sudden shifts of SA-CASSCF energies); 11 of these were on  $S_0$ , 5 on  $S_1$  and 2 on  $S_2$ . All such failed trajectories were restarted from time zero with a reduced time step of 0.25 fs; all but one of the new trajectories successfully reached 200 fs. Out of all the 136 trajectories, 9 have remained on  $S_1$  by the end of the 200 fs simulation time, although some showed a significant trend towards dissociation. This output, together with the recent experimental evidence that the outcome of reaction for vibrationally-hot molecules may not be decided within such a short time frame,<sup>11</sup> led us to continue dynamics for another 200 fs for all the successful trajectories, using the same step sizes as in the first 200 fs i.e. 0.5 fs and 0.25 fs for the initially successful and unsuccessful trajectories correspondingly. By the end of the 400 fs simulation time, as many as 24 trajectories (18%) failed to conserve the total energy (1 trajectory between 100 and 200 fs, 7 between 200 and 300 fs and 16 between 300 and 400 fs; some of which were from the 0.5 fs- and some from the 0.25 fs-step pool), however

all trajectories ended up on  $S_0$  with a clear separation into the HT and CHD molecules photoproducts (we here consider all geometries with  $r(C_1 - C_6) \geq 3.0 \text{ \AA}$  to fall into the HT product pool), and so we used all of them for the analysis. The resulting QY for HT formation was  $47 \pm 8\%$  (64 trajectories out of 136), where the margin of error was estimated for a 95% interval of confidence. Such a margin does not allow us to conclude from our calculations that the QY is skewed towards the reactant. However, some of the features of the reaction mechanism described below may speak in favor of this hypothesis.

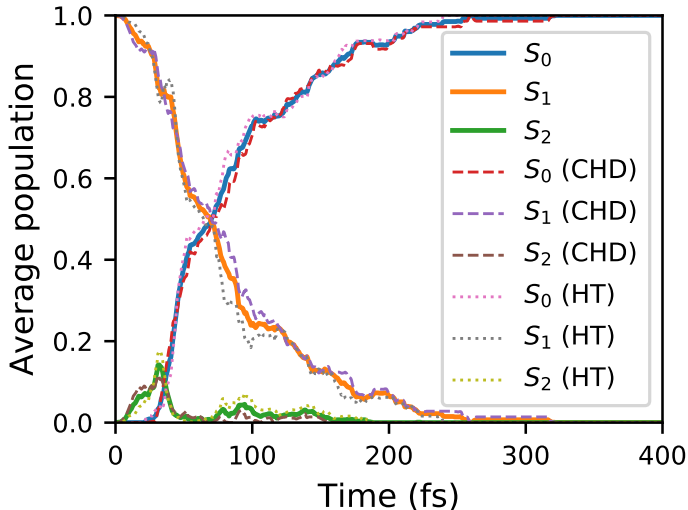


Figure 5: Average adiabatic population of the three electronic states involved in the reaction. Solid lines represent total population, while dashed and dotted lines represent population calculated for the trajectories that end up conserving the ring and the trajectories proceeding to dissociation correspondingly. For the crashed trajectories, their final population (always at  $S_0$ ) has been propagated till the 400 fs.

Fig. 5 shows the average adiabatic population evolution on all the three electronic states involved in the dynamics, calculated both for the total ensemble of trajectories as well as separately for the subsets of trajectories that end up either breaking or conserving the ring correspondingly. There is nearly no difference in the rates of population transfer for the two reaction channels, and so the following discussion concerns any of the three representations.

There is a clear peak of population in  $S_2$  in the first 50 fs, which overlaps with the onset of population growth on the ground state, starting at  $\sim 25$  fs. Since (along the symmetry-

conserving coordinate) at the  $S_2/S_1$  MECI the  $1^1B$  diabatic state becomes the  $S_2$  adiabatic state, this peak is most easily explained as the proportion of the nuclear wavepacket staying on the same diabatic state and then oscillating back towards the CoIn seam with  $2^1A$ . However, as shown below, the spread of geometries at the  $S_1 \leftrightarrow S_2$  hops is rather broad and not centered around the  $S_2/S_1$  MECI geometry, so  $1^1B \leftrightarrow 2^1A$  hops are also possible. Later, there are two smaller recurring peaks of  $S_2$  population, centred at 95 and 138 fs.

Decay of the  $S_1$  and growth of the  $S_0$  population are rather steep, with 93% of population being on  $S_0$  by 200 fs and 100% of trajectories being on  $S_0$  by 322 fs. We estimated the constants  $\tau^{S_1}$  of  $S_1$  population decay and  $\tau^{S_0}$  of  $S_0$  population growth to be  $72 \pm 9$  fs and  $73 \pm 9$  fs correspondingly, by performing monoexponential fits to  $N^{S_1} = e^{-(t-t_0^{S_1})/\tau^{S_1}}$  and  $N^{S_0} = 1 - e^{-(t-t_0^{S_0})/\tau^{S_0}}$  respectively, and using the bootstrap approach<sup>58</sup> to estimate the margins of error for the 95% confidence interval. The corresponding latency time parameters were  $t_0^{S_1} = 12 \pm 2$  fs and  $t_0^{S_0} = 16 \pm 2$  fs. By noting that the  $S_0$  population growth constants are complimentary to the overall excited states population decay constants, we estimate the excited lifetime as  $\tau^{S_0} + t_0^{S_0} = 89 \pm 9$  fs.

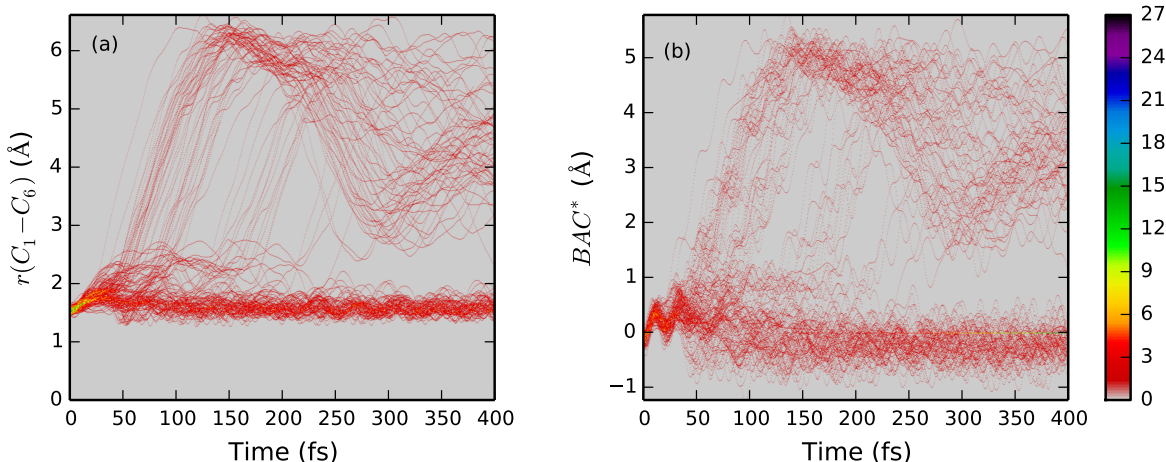


Figure 6:  $C_1 - C_6$  interatomic distance and BAC\* evolution heat map for the ensemble of 136 trajectories. For atom labeling, see Fig. 3.

Fig. 6 depicts the time evolution both of the  $C_1 - C_6$  interatomic distance, as well as the

extended bond alternation coordinate (BAC\*), which we define as  $r(C_2 - C_3) + r(C_4 - C_5) - r(C_1 - C_2) - r(C_5 - C_6) - r(C_3 - C_4) + r(C_1 - C_6)$  in accordance with Schalk et al.,<sup>28</sup> which reflects both the oscillation of the diene moiety and the ring-opening dynamics. As early as around 25 fs, in some trajectories, the  $C_1 - C_6$  bond starts sharp elongation leading to a fast dissociation, in some other it oscillates at around  $2 - 2.5 \text{ \AA}$  for the next 100 – 150 fs before either proceeding towards dissociation or falling back to the covalent bond distance, while in the rest of trajectories it keeps oscillating around its equilibrium length during the whole simulation time. After 250 fs no more trajectories exhibit ring-opening motion and one can clearly separate them into the CHD and HT pools. The dissociative trajectories appear to exhibit a large-amplitude oscillation for  $r(C_1 - C_6)$ , which for many of them becomes shorter again in the course of dynamics (to as low as  $2.5 \text{ \AA}$ ), but never falls back to the covalent bond length and tends to oscillate again to a larger interatomic distance at long time.

The large-amplitude oscillation of the  $C_1 - C_6$  interatomic distance can be explained by looking at the time evolution of the carbon ring dihedral angles as depicted in Fig. 7. Specifically, the  $\sphericalangle C_1 C_2 C_3 C_4$  and  $\sphericalangle C_6 C_5 C_4 C_3$  dynamics (Fig. 7 (b,c)) is of most interest. One can see that for a large subset of trajectories both of those angles undergo a nearly  $360^\circ$  rotation (we note that rotation is conrotatory in accordance with the Woodward-Hoffmann rule - the same sign here is due to the order of atoms in which the angles are being evaluated). One can make a conclusion that in some of the trajectories producing HT, the vibrational modes leading to dissociation gain enough momentum to continue the conrotatory motion of the broken ring such that it can make a full cycle and end up in a configuration close to the inverted reactant. It is important to note, however, that no bond formation has been detected by the end of a 400 fs simulation, according to Fig. 6.

Fig. 7 (a) and (d) show somewhat less intriguing dynamics, with the  $\sphericalangle C_1 C_3 C_4 C_6$  also showing some large-amplitude motion, but to a much smaller extent, and  $\sphericalangle C_2 C_3 C_4 C_5$  oscillating within an approximate range of  $[-75^\circ, +75^\circ]$  with some larger deviations further along the dynamics.

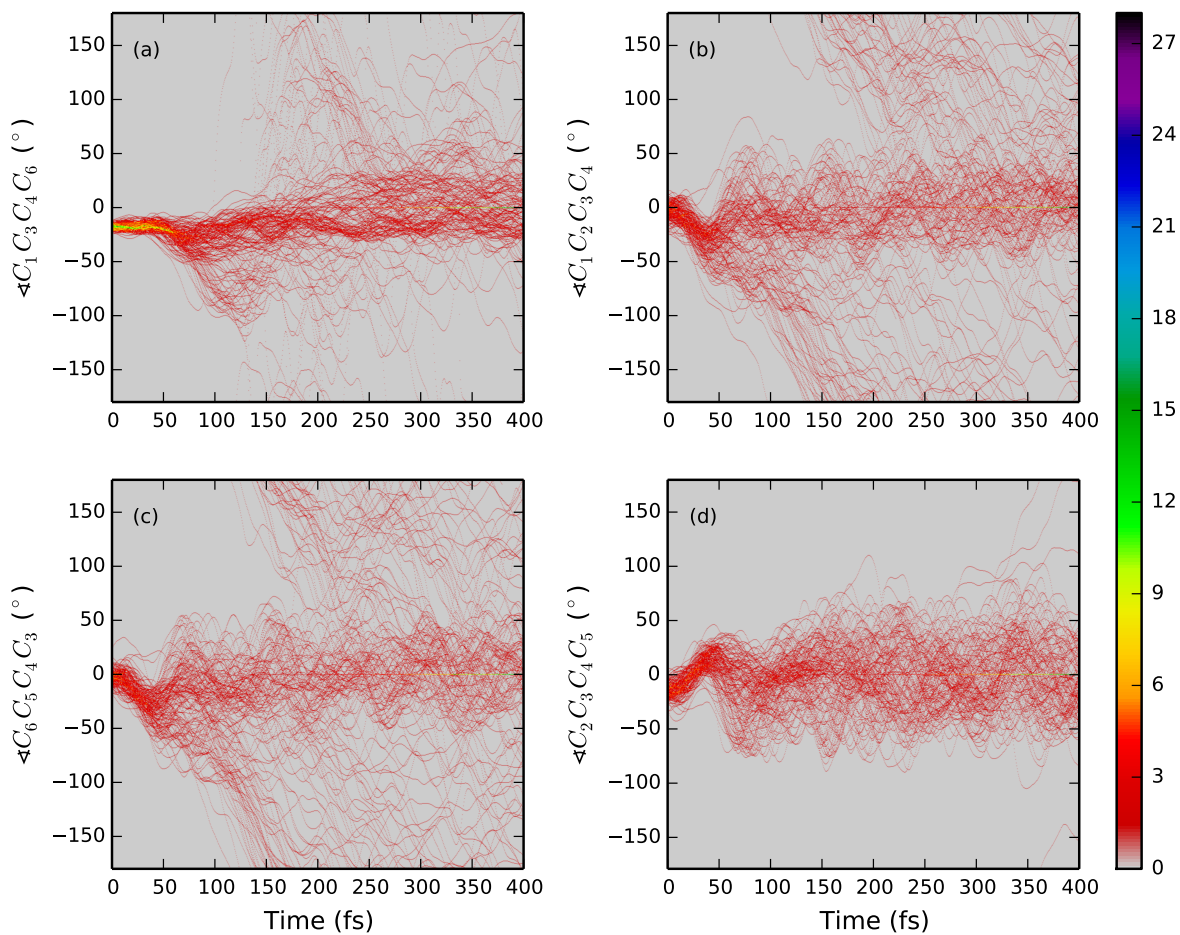


Figure 7: The four carbon chain dihedral angles evolution heat map for the ensemble of 136 trajectories. For atom labeling, see Fig. 3. Horizontal line at the zero value of each angle visible by the end of simulation time is due to trajectories that crashed prematurely.

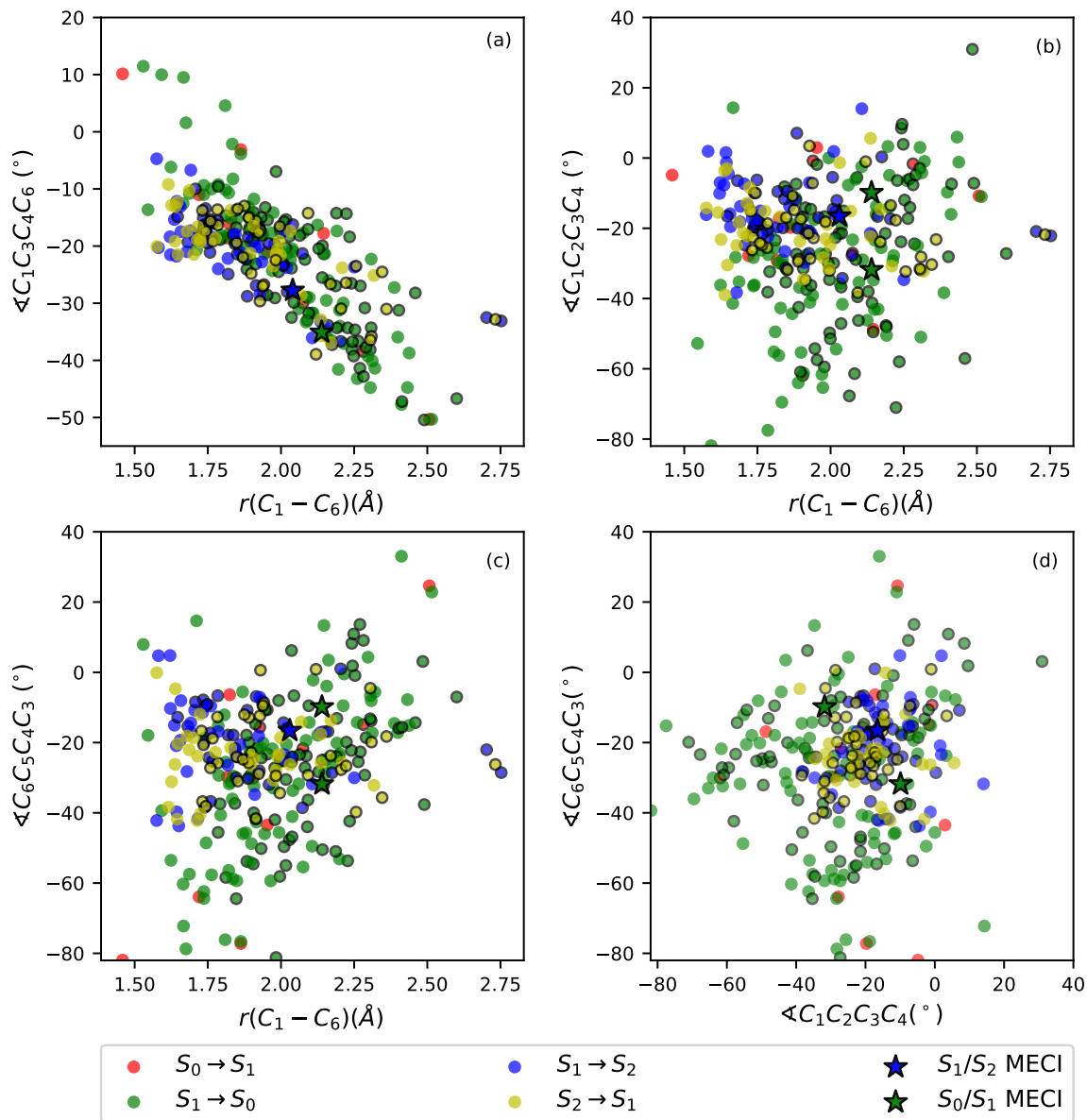


Figure 8: Distribution of geometries undergoing non-adiabatic transitions during the 400 fs dynamics for the ensemble of 136 trajectories. Differently colored circles designate transitions between different pairs of states. Circles with black border belong to the dissociating trajectories while borderless circles belong to the ring-conserving trajectories. Stars label the MECI geometries (two values are plotted for the  $S_0/S_1$  MECI on (b-d) due to the  $C_2$ -symmetry of the equilibrium geometry). For atom labeling, see Fig. 3.

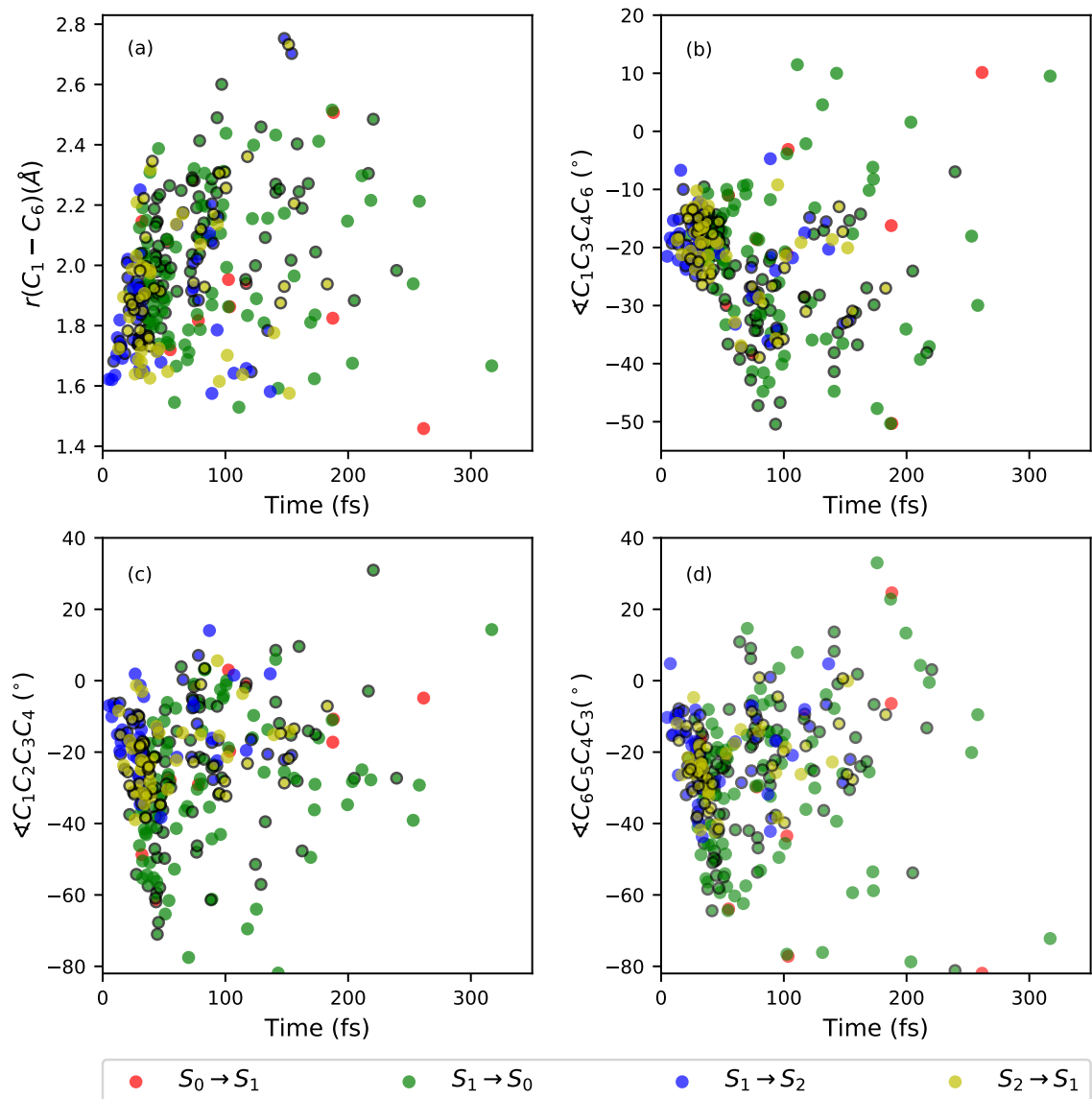


Figure 9: Distribution of geometries undergoing non-adiabatic transitions with respect to time during the 400 fs dynamics for the ensemble of 136 trajectories. Differently colored circles designate transitions between different pairs of states. Circles with black border belong to the dissociating trajectories while borderless circles belong to the ring-conserving trajectories. For atom labeling, see Fig. 3.

The distribution of geometries at which the transitions (hops) between the various electronic states occur in the course of dynamics for the whole ensemble of trajectories, as well as the reaction outcome (whether proceeding to dissociation or not), are depicted in Fig. 8 (a-d) in the form of the four different 2D projections in coordinate space. Importantly, we notice that all the projections reveal a highly-dispersed nature of the hops between any pair of the three states involved, with the  $S_1 \leftrightarrow S_2$  transitions being on average more localized (at shorter  $r(C_1 - C_6)$  and smaller carbon ring dihedral angles) compared to the  $S_1 \rightarrow S_0$  transitions that are spread out to much larger structural distortions. Furthermore, there is nearly no correlation of the positions in coordinate space at which transitions occur with respect to the outcome of reaction. The only visible trend is that while trajectories conserving the ring may hop at any  $C_1 - C_6$  interatomic distance, those proceeding to dissociation must undergo the  $S_1 \rightarrow S_0$  hops (and, more surprisingly, in majority of cases even the  $S_1 \leftrightarrow S_2$  hops) at  $r(C_1 - C_6) > 1.75 \text{ \AA}$ . This trend may, however, be quite important for the outcome of reaction, and while our calculations can not provide an unbiased support for the hypothesis of a QY skewed in favor of the reactant, as we discuss later, it could be one of the main mechanistic causes for it. We note that in our simulations we also observed several  $S_0 \leftrightarrow S_2$  hops, but they are omitted from the plot for clarity, as they do not seem to provide any valuable information regarding the reaction mechanism.

The two mostly informative projections are the  $r(C_1 - C_6)/\langle C_1 C_3 C_4 C_6 \rangle$  (Fig. 8 (a)) and  $\langle C_1 C_2 C_3 C_4 \rangle / \langle C_6 C_5 C_4 C_3 \rangle$  (Fig. 8 (d)). By looking at Fig. 8 (a), one can make two important observations. Firstly, most of the  $S_1 \rightarrow S_2$  and  $S_2 \rightarrow S_1$  transitions happen at lower  $r(C_1 - C_6)$  and  $\langle C_1 C_3 C_4 C_6 \rangle$  values (closer to equilibrium) compared to the  $S_1/S_2$  MECI. Secondly, both MECIs lie close to the lower border of the hops distribution, having one of the lowest (highest negative) values of  $\langle C_1 C_3 C_4 C_6 \rangle$  for a given value of  $r(C_1 - C_6)$ . It is therefore reasonable to talk about extended seams of intersections along which population transfer may occur during dynamics, both between  $S_1$  and  $S_0$  and between  $S_1$  and  $S_2$ .

Fig. 8 (d) would ideally show a symmetric distribution of hop geometries with respect to

the  $x = y$  (diagonal) axis. One can again notice a more clustered distribution of  $S_1 \leftrightarrow S_2$  hops at the centre of the plot (and close to the  $S_1/S_2$  MECI geometry) and a more spread distribution of  $S_1 \rightarrow S_0$  transitions, with higher density at asymmetric molecular geometries featuring different values for the two equivalent dihedral angles, in accordance with the  $S_0/S_1$  MECI geometries.

Finally, the distributions of the same set of internal coordinates at the non-adiabatic transitions with respect to time are presented at Fig. 9 (a-d). We do not observe any correlation between the time at which the hops happen and the outcome of reaction. Regarding the type of transition though, one can clearly see that initially only the  $S_1 \rightarrow S_2$  and  $S_2 \rightarrow S_1$  transitions occur, then there is a well-defined cluster of  $S_1 \rightarrow S_0$  hops approximately between 35 and 70 fs, and then another thin cluster of  $S_1 \rightarrow S_2$  and  $S_2 \rightarrow S_1$  transitions between 70 and 100 fs, after which mainly the transitions to the ground state occur, totally in accordance with Fig. 5.

## 4 Discussion

In the current work we estimate the excited states lifetime to be  $89 \pm 9$  fs, consisting of a monoexponential population decay constant of  $73 \pm 9$  fs and a latency time of  $16 \pm 2$  fs, which is a somewhat faster rate compared to the most of the estimations that have been derived from experiments up to now. The latter rather consistently describe the excited-state lifetime in terms of the two consecutive exponentially decaying processes with the constants of 30 – 70 fs and 60 – 80 fs, commonly ascribed to the lifetimes of the  $1^1B$  and  $2^1A$  states correspondingly, usually adding up to the total excited-state lifetime of 130 – 140 fs.<sup>5-11</sup> Only one recent X-ray scattering experiment gave a lower estimation of 80 fs as a time constant for the whole structural part of the CHD  $\rightarrow$  HT transformation,<sup>32</sup> while the two other recent studies, employing X-ray absorption spectroscopy and electron diffraction, provided somewhat broader estimates of  $170 \pm 80$ <sup>34</sup> and  $110 \pm 30$  fs,<sup>33</sup> respectively. Unfortunately, it

is not an easy task to calculate the diabatic state populations in a non-adiabatic dynamics study, but we can probably roughly estimate the upper bound for the lifetime of  $1^1B$  state by the maximum of  $S_2$  population, located in this work approximately at 30 fs (see Fig. 5). The latency time of 10–21 fs, commonly attributed to the time that takes the wavepacket to leave the FC region, has also been estimated in experiments previously.<sup>5-7,9</sup> Thus, constants resulting from our fit correspond to the lowest reported rate estimates.

A possible underestimation of the excited-state lifetime may be due to a slightly higher than experimental vertical excitation energy at the equilibrium geometry as given by the XMS-CAS(6,6)PT2 and a cc-pVDZ basis set (5.13 eV in the current work *vs* 4.94 eV in experiment,<sup>16</sup> see also absorption spectra maxima in Fig. 4), resulting in a slightly steeper slope along the  $1^1B$  and/or the  $2^1A$  states, which may artificially accelerate the dynamics.

The QY of  $47 \pm 8\%$  obtained in this work is somewhat higher than the recently reported value of  $30\%$ <sup>11</sup> (which should however be noted to be an estimation obtained from a fit rather than a directly measured property) as well as the original value of  $40\%$  reported for condensed phases. Apart from a relatively large margin of error due to a finite number of trajectories, our result is based on a 400 fs-only dynamics simulation, and, while probably unlikely, there is a chance that some of the vibrationally-hot trajectories may have returned to the CHD conformation at later stages. Also, a higher QY may also be related to the steeper slope on the excited states, as will be explained below.

Further, our results in many parts differ from the four fully-dimensional surface hopping dynamics calculations published up to now.<sup>27-30</sup> While three of them provide similar excited state lifetime estimates,<sup>27-29</sup> each of those studies describes a mechanism of CHD photodissociation somewhat different to what we see in our study. We consider now these earlier works in more detail and compare them to our results, in order to draw an updated picture of the reaction mechanism. The main characteristics of these works are also summarized and compared to our results in Table 2 for easier reference.

Schalk et al.<sup>28</sup> in their LR-TD-DFT surface hopping study, accounting for only  $S_1$  and  $S_0$

Table 2: Comparison of CHD photodissociation surface hopping studies

	This work	Ohta <i>et al.</i> <sup>27,a</sup>	Lei <i>et al.</i> <sup>29</sup>	Schalk <i>et al.</i> <sup>28</sup>	Filatov <i>et al.</i> <sup>30</sup>
PES description	XMS-CAS(6,6)PT2/ cc-pVDZ	MS-MR-CAS(8,8)PT2/ cc-pVDZ	SA-CAS(14,8)SCF/ 6-31G*	LR-TD-PBE0/ def2-SVP	SSR- $\omega$ PBEh/ 6-31G*
NACs description	XMS-CAS(6,6)PT2/ cc-pVDZ	SA-CAS(8,8)SCF/ cc-pVDZ	SA-CAS(14,8)SCF/ 6-31G*	LR-TD-PBE0/ def2-SVP	SSR- $\omega$ PBEh/ 6-31G*
Hopping algorithm	DC-FSSH <sup>b</sup>	ZN <sup>c</sup>	ZN	FSSH	DISH-XF <sup>d</sup>
Electronic states involved	$S_0, S_1, S_2$	$S_0, S_1, S_2$	$S_0, S_1, S_2$	$S_0, S_1$	$S_0, S_1$
Duration of simulations (fs)	400	> 600	500	5000	500
# of trajectories	136	42	600	119	50
$\tau^{S_1}$ equiv. (fs)	$72 \pm 9$	47	$82^e$	52	$234 \pm 8$
$t_0^{S_1}$ equiv. (fs)	$12 \pm 2$	21		29	$43 \pm 5$
QY (%HT) <sup>f</sup>	$47 \pm 8$	$40 \pm 15$	$47 \pm 4$	$64 \pm 9$	$36 \pm 13$

<sup>a</sup> We only report here results of trajectories initiated on  $S_1$ ; <sup>b</sup> decoherence corrected fewest switches surface hopping; <sup>c</sup> Zhu-Nakamura formula; <sup>d</sup> decoherence-induced surface hopping based on the exact factorization; <sup>e</sup>  $\tau^{S_1} + t_0^{S_1}$  is reported; the adiabatic population shown in Fig. 7a in Ref. [29] however does not decay monoexponentially, so the fit should be addressed carefully; <sup>f</sup> the margin of error in each case was computed for 95% confidence interval.

states, report different decay rates for the dissociative and ring-conserving trajectories. The authors conclude that nearly all trajectories that have higher velocities along the positive BAC and  $r(C_1 - C_6)$  displacements proceed towards dissociation within the first 100 fs, while those that remain on the excited state by that time cannot any more gain enough velocity to successfully open the ring, and slowly decay to a closed configuration. On the contrary, we have not observed any significant differences in the rates for the dissociative and ring-conserving trajectory ensembles (see Fig. 5), and further show that there is no correlation between the times at which hops between states occur and the outcome of reaction. Our results are, however, consistent with the notion that the driving force behind the dissociative outcome must be the momentum gained along the  $C_1 - C_6$  bond elongation, but our calculations also suggest that it can be gained even after a few cycles of the bond vibrating

on the excited states. The QY reported by Schalk *et al.*,  $64 \pm 9\%$ , is an outlier value, falling above the upper limit of the QY predicted by all other SH simulations reported in Table 2. Such a qualitatively different result seems to point out to either some fundamental limitation of linear-response TD-DFT to describe the  $S_0/S_1$  crossing seam, even when analytic NACs are used, or the necessity to explicitly include the  $S_2$  state in dynamic calculations, or both. Importantly, in our calculations we see that the double excitation character of  $2^1A$  is still an important contribution to the nature of both excited states at the  $S_1/S_2$  MECI geometry as well as later in the course of reaction, which can not be described by LR-TD-DFT.

Lei *et al.*<sup>29</sup> employ CASSCF with a somewhat unbalanced active space of 14 electrons in 8 orbitals containing only a single virtual orbital, which however provides them with the right  $S_1/S_2$  state ordering at the FC point. They also observe the two distinct phases of the reaction, albeit having a different nature. Their electronic state population evolution bears a quasi-two-step character, with the first phase mainly constituted from the  $S_1 \leftrightarrow S_2$  population transfer and only slight increase in  $S_0$  population, followed by a plateau, and then a rather steep  $S_1 \rightarrow S_0$  population decay. While we also see  $S_1 \leftrightarrow S_2$  transitions first, followed by a cluster of  $S_1 \rightarrow S_0$  hops (Fig. 9), alternation happens much faster and in a much more diffuse way, ensuring a smooth overall monoexponential decay of  $S_1$  and rise of  $S_0$  populations.

Ohta *et al.*<sup>27</sup> use MS-CASPT2 energies and gradients (however also employing a somewhat unbalanced active space, containing an asymmetric set of two  $\sigma, \sigma^*$ -orbital pairs) in their surface hopping calculations, but employ the semi-classical Zhu-Nakamura formula to calculate the transition probabilities from the SA-CASSCF NACs. Although Zhu-Nakamura surface hopping has been shown to deliver results of similar quality as those obtained with the fewest-switches surface hopping for a specific case,<sup>59</sup> the model is in principle only valid for surface crossings with a Landau-Zener-like topography. For this reason, when dealing with a complex non-adiabatic topography like in the present case, it is desirable to resort to a more general algorithm, such as DC-FSSH. They obtain a smooth monoexponential

decay of  $S_1$  population with the constant of 47 fs and a latency of 21 fs, giving a similar but somewhat faster rate compared to our result. The faster lifetime can be partially explained by a significantly overestimated  $S_0 \rightarrow S_1$  vertical excitation at the FC point, and, accordingly, artificially steep slopes of excited states. The authors do not distinguish fast- and slow-decaying trajectories; rather, based on a plot similar to Fig. 8 (a) they conclude that the ring-conserving trajectories hit the  $S_1/S_0$  CI seam at the shorter values of  $r(C_1 - C_6)$ , while the majority of trajectories that decay to  $S_0$  at a longer bond length, proceed to dissociation. In our calculations, we confirm that all of the trajectories hitting the  $S_1/S_0$  seam at  $r(C_1 - C_6) < 1.75 \text{ \AA}$  end up conserving the ring. However, we did not find any correlation between the geometries at which transitions happen and the outcome of reaction at longer  $r(C_1 - C_6)$  values. Still, while the QY obtained from our calculations (as well as the QY obtained by Ohta *et al.* - see margins of error provided in Table 2) can not confirm the reaction outcome being skewed in favor of the preserved ring (as the recent experiments suggest), the fact that only the trajectories undergoing the  $S_1 \rightarrow S_0$  hops at  $r(C_1 - C_6) > 1.75 \text{ \AA}$  have a chance to proceed towards ring opening, may in fact be one of the reasons for it.

Finally, Filatov *et al.*<sup>30</sup> recently employed the SSR method that allows to treat the  $S_0/S_1$  CI in a more rigorous way compared to conventional single-reference TD-DFT. Still only considering the two lowest electronic states in their decoherence-induced, exact factorization-based surface hopping dynamics study, they obtain a rather slow  $S_1$  population decay which they fit to a monoexponential function obtaining the decay constant of  $234 \pm 8$  fs and a latency of  $43 \pm 5$  fs. The authors argue that this result corresponds well to the rates reported by Adachi *et al.*<sup>11</sup> where the  $1^1B/2^1A$  and  $2^1A/1^1A$  internal conversion time constants were estimated to be  $70 \pm 10$  and  $60 \pm 20$  fs correspondingly, followed however by an approximately 100 fs delay before the rise in both the CHD and HT signatures (giving in total  $230 \pm 30$  fs before the  $S_0$  population rise), which Adachi *et al.* attributed to the “time required for wavepacket motion from  $2A$  state to the  $1A$  state” without giving any possible mechanistic explanation for this statement. We find such comparison of time constants rather ambiguous,

especially since Pemberton et al.<sup>10</sup> have in the same year reported a much more conventional estimate of 142 fs for the product formation rate. Apart from that, Filatov et al. provide mechanistic interpretation of the photoexcited dissociation of CHD that agrees well with what we see in our study. They do not find any correlation between the  $C_1 - C_6$  interatomic distance at the geometries of surface hops and the outcome of reaction (except for  $r(C_1 - C_6) < 1.8 \text{ \AA}$ , where, again, all trajectories end up conserving the ring). Instead, they find that trajectories achieving a certain synchronization between the displacements along specific vibrational modes gain sufficient momentum along the  $C_1 - C_6$  stretching coordinate (while still being at the  $S_1$  state) and end up at the dissociated HT product conformation. This finding is further supported in a separate work,<sup>42</sup> where by analysing the electron density along the minimum energy ring-opening reaction path using the quantum theory of atoms in molecules (QTAIM), the authors demonstrate that due to an attractive interaction between the ends of the  $C_1 - C_6$  bond that by default steers the reaction towards the restoration of the CHD structure, ring opening can only be achieved when there is a sufficient nuclear momentum in the direction of the bond stretching. They use this finding to explain the experimentally- and computationally-observed QY of  $< 50\%$ . While we do not directly analyse interplay between specific vibrational modes and their momentum at the interstate transitions, lack of correlation between the values of the carbon ring internal coordinates at the corresponding geometries and the outcome of reaction strongly supports the idea of the sufficient momentum gained along the bond-breaking coordinate being the driving force behind the molecule choosing dissociation path upon decaying to the ground state. At shorter values of  $r(C_1 - C_6)$ , the trajectories (portion of the nuclear wavepacket) that decay to  $S_0$  may never have enough momentum in the right direction, thereby possibly contributing to the skewing of the QY towards the CHD configuration (yet again, the resulting QY obtained in current work can not be interpreted as skewed).

We further note that full-dimensional wavepacket-based AIMS<sup>26,33,44,45</sup> and *ab initio* multiconfigurational Ehrenfest (AI-MCE)<sup>31,32,60</sup> calculations, based on SA3-CAS(6,4)SCF or

(empirically-corrected) SA2- $\alpha$ -CAS(6,4)SCF<sup>33</sup> surfaces, have been also performed, mainly in support of experimental studies and with less emphasis on obtaining converged kinetic characteristics such as QY or excited states lifetime. Nevertheless, some of those studies provide results that can be compared to current work. In Refs. 44 and 26, the field-induced non-adiabatic transitions are mainly studied, but in the latter work a 1 : 1 ratio of closed- to open-ring final products is reported for the field-free photodissociation. In Refs. 31 and 32, just a few AI-MCE trajectories (of both the ring-opening and ring-conserving types) are shown to be enough to fit experimental X-ray scattering signatures to a good precision, but neither QY values nor lifetime constants are estimated. In Ref. 60, following the similar logic, four out of a hundred of AI-MCE 200 fs-long trajectories are used to compute time-resolved photoelectron spectra and study effects of various probe pulses and competing pathways on predicted signals. Adiabatic population evolution is calculated for those four trajectories, which can hardly be characterized by a monoexponential decay, with neither  $S_1$  nor  $S_2$  states getting completely depopulated by 200 fs, and no time constants are reported. Finally, in a recently published electron diffraction study,<sup>33</sup> a 500 fs  $\alpha$ -CAS(6,4)SCF AIMS calculation, including only  $S_0$  and  $S_1$  states, is reported. Being primarily used to evaluate structural signatures (atomic difference pair distribution functions) to be compared to experimental results, it also reports the (somewhat slower compared to the current study) adiabatic population evolution and an estimated  $S_1$  state lifetime of  $139 \pm 25$  fs (where the 99% confidence interval was used to compute the margins of error). To justify the inclusion of only two electronic states in their calculations, the authors check (as given in the Supplementary Material) for differences in adiabatic population evolution when  $S_2$  state is included. They come to a conclusion that the differences can be neglected; however, we note that in their three state calculation, while the  $S_2$  state is populated much later and to a much lesser extend than in our calculations, the associated  $S_1$  state depopulation starts later, and reaches near-depletion earlier, compared to their two-state calculation.

In this way, results of the current work differ in some aspects and are similar in other

aspects to the other existing full-dimensional non-adiabatic dynamics studies, hopefully providing a more consistent understanding of the mechanism behind this photoreaction. As a final remark, we would like to note that a broad distribution of geometries at which interstate transitions occur in the current work favours the idea of an extended CI seam proposed by Nenov et al.<sup>19</sup> (not only between  $S_0$  and  $S_1$  however, but also between  $S_1$  and  $S_2$ ), which contributes to the QY as discussed above.

## 5 Conclusions

We performed a non-adiabatic dynamics study of the photo-dissociation of 1,3-cyclohexadiene, an important problem in photochemistry. For the first time, a balanced high-level treatment of dynamics and electronic structure was achieved, combining the full dimensionality of mixed quantum-classical approaches, the generality of the decoherence-corrected fewest switches surface hopping, significant statistical ensembles, proper account of initial conditions, and the state-of-the-art quality of the XMS-CASPT2 energies, energy gradients, and non-adiabatic couplings. We estimate the excited lifetime to be  $89 \pm 9$  fs, consisting of a  $16 \pm 2$  fs latency and  $73 \pm 9$  fs decay time constant, corresponding to the lowest rate observations among the experiments. The calculated quantum yield for the dissociated product is  $47 \pm 8\%$ . Having mapped out an extended conical intersection seam along the reaction coordinate, we observe no correlation between the values of the carbon ring internal coordinates at the geometries undergoing non-adiabatic transitions and the outcome of reaction, except for the lower values of the  $C_1 - C_6$  interatomic distance. We conclude that the momentum gained along the bond breaking coordinate ensures the dissociative outcome at its larger values, while for transitions happening closer to the equilibrium geometry the outcome is always conservation of the ring.

## Acknowledgement

IP acknowledges the support of the Supercomputing Wales project, which is part-funded by the European Regional Development Fund (ERDF) via Welsh Government.

MB thanks the support of the Excellence Initiative of Aix-Marseille University (A\*MIDEX) and the project Equip@Meso (ANR-10-EQPX-29-01), both funded by the French Government “Investissements d’Avenir” program. MB also acknowledges funding from the WSPLIT project (ANR-17-CE05-0005-01).

## Supporting Information Available

Cartesian coordinates for the CHD ground state minimum energy,  $S_1/S_2$  and  $S_0/S_1$  MECI geometries, the multiple fits to the  $S_0$  average adiabatic population, obtained via the bootstrapping approach in order to estimate the mean values and margins of error for the time constants, final distributions and time evolution of the relative total energies for all trajectories simulated, as well as details on computational costs. This material is available free of charge via the Internet at <http://pubs.acs.org/>.

## References

- (1) Arruda, B. C.; Sension, R. J. Ultrafast Polyene Dynamics: the Ring Opening of 1,3-Cyclohexadiene Derivatives. *Phys. Chem. Chem. Phys.* **2014**, *16*, 4439–4455.
- (2) Woodward, R. B.; Hoffmann, R. The Conservation of Orbital Symmetry. *Angew. Chem. Int. Ed.* **1969**, *8*, 781.
- (3) van der Lugt, W. T. A. M.; Oosterhoff, L. J. Symmetry Control and Photoinduced Reactions. *J. Am. Chem. Soc.* **1969**, *91*, 6042–6049.
- (4) Deb, S.; Weber, P. M. The Ultrafast Pathway of Photon-Induced Electrocyclic Ring-

- Opening Reactions: The Case of 1,3-Cyclohexadiene. *Annu. Rev. Phys. Chem.* **2011**, *62*, 19–39.
- (5) Trushin, S. A.; Fuß, W.; Schikarski, T.; Schmid, W. E.; Kompa, K. L. Femtosecond Photochemical Ring Opening of 1,3-Cyclohexadiene Studied by Time-Resolved Intense-Field Ionization. *J. Chem. Phys.* **1997**, *106*, 9386–9389.
- (6) Fuß, W.; Schmid, W. E.; Trushin, S. A. Time-Resolved Dissociative Intense-Laser Field Ionization for Probing Dynamics: Femtosecond Photochemical Ring Opening of 1,3-Cyclohexadiene. *J. Chem. Phys.* **2000**, *112*, 8347–8362.
- (7) Garavelli, M.; Page, C. S.; Celani, P.; Olivucci, M.; Schmid, W. E.; Trushin, S. A.; Fuss, W. Reaction Path of a sub-200 fs Photochemical Electrocyclic Reaction. *J. Phys. Chem. A* **2001**, *105*, 4458–4469.
- (8) Kuthirummal, N.; Rudakov, F. M.; Evans, C. L.; Weber, P. M. Spectroscopy and Femtosecond Dynamics of the Ring Opening Reaction of 1,3-Cyclohexadiene. *J. Chem. Phys.* **2006**, *125*, 133307.
- (9) Kosma, K.; Trushin, S. A.; Fuß, W.; Schmid, W. E. Cyclohexadiene Ring Opening Observed with 13 fs Resolution: Coherent Oscillations Confirm the Reaction Path. *Phys. Chem. Chem. Phys.* **2009**, *11*, 172–181.
- (10) Pemberton, C. C.; Zhang, Y.; Saita, K.; Kirrander, A.; Weber, P. M. From the (1B) Spectroscopic State to the Photochemical Product of the Ultrafast Ring-Opening of 1,3-Cyclohexadiene: A Spectral Observation of the Complete Reaction Path. *J. Phys. Chem. A* **2015**, *119*, 8832–8845.
- (11) Adachi, S.; Sato, M.; Suzuki, T. Direct Observation of Ground-State Product Formation in a 1,3-Cyclohexadiene Ring-Opening Reaction. *J. Phys. Chem. Lett.* **2015**, *6*, 343–346.

- (12) Celani, P.; Ottani, S.; Olivucci, M.; Bernardi, F.; Robb, M. A. What Happens during the Picosecond Lifetime of  $2A_1$  Cyclohexa-1,3-diene? A CAS-SCF Study of the Cyclohexadiene/Hexatriene Photochemical Interconversion. *J. Am. Chem. Soc.* **1994**, *116*, 10141–10151.
- (13) Celani, P.; Bernardi, F.; Robb, M. A.; Olivucci, M. Do Photochemical Ring-Openings Occur in the Spectroscopic State?  $^1B_2$  Pathways for the Cyclohexadiene/Hexatriene Photochemical Interconversion. *J. Phys. Chem.* **1996**, *100*, 19364–19366.
- (14) Garavelli, M.; Celani, P.; Fato, M.; Bearpark, M. J.; Smith, B. R.; Olivucci, M.; Robb, M. A. Relaxation Paths from a Conical Intersection: The Mechanism of Product Formation in the Cyclohexadiene/Hexatriene Photochemical Interconversion. *J. Phys. Chem. A* **1997**, *101*, 2023–2032.
- (15) Garavelli, M.; Bernardi, F.; Olivucci, M.; Vreven, T.; Klein, S.; Celani, P.; Robb, M. A. Potential-Energy Surfaces for Ultrafast Photochemistry. Static and Dynamic Aspects. *Faraday Discuss.* **1998**, *110*, 51–70.
- (16) Merchán, M.; Serrano-Andrés, L.; Slater, L. S.; Roos, B. O.; McDiarmid, R.; Xing, X. Electronic Spectra of 1,4-Cyclohexadiene and 1,3-Cyclohexadiene: A Combined Experimental and Theoretical Investigation. *J. Phys. Chem. A* **1999**, *103*, 5468–5476.
- (17) Tamura, H.; Nanbu, S.; Nakamura, H.; Ishida, T. A Theoretical Study of Cyclohexadiene/Hexatriene Photochemical Interconversion: Multireference Configuration Interaction Potential Energy Surfaces and Transition Probabilities for the Radiationless Decays. *Chem. Phys. Lett.* **2005**, *401*, 487–491.
- (18) Mori, T.; Kato, S. Dynamic Electron Correlation Effect on Conical Intersections in Photochemical Ring-Opening Reaction of Cyclohexadiene: MS-CASPT2 Study. *Chem. Phys. Lett.* **2009**, *476*, 97–100.

- (19) Nenov, A.; Kölle, P.; Robb, M. A.; de Vivie-Riedle, R. Beyond the van der Lugt/Oosterhoff Model: When the Conical Intersection Seam and the  $S_1$  Minimum Energy Path Do Not Cross. *J. Org. Chem.* **2010**, *75*, 123–129.
- (20) Hofmann, A.; de Vivie-Riedle, R. Quantum Dynamics of Photoexcited Cyclohexadiene Introducing Reactive Coordinates. *J. Chem. Phys.* **2000**, *112*, 5054–5059.
- (21) Hofmann, A.; de Vivie-Riedle, R. Adiabatic Approach for Ultrafast Quantum Dynamics Mediated by Simultaneously Active Conical Intersections. *Chem. Phys. Lett.* **2001**, *346*, 299–304.
- (22) Tamura, H.; Nanbu, S.; Ishida, T.; Nakamura, H. Ab Initio Nonadiabatic Quantum Dynamics of Cyclohexadiene/Hexatriene Ultrafast Photoisomerization. *J. Chem. Phys.* **2006**, *124*, 084313.
- (23) Schönborn, J. B.; Sielk, J.; Hartke, B. Photochemical Ring-Opening of Cyclohexadiene: Quantum Wavepacket Dynamics on a Global Ab Initio Potential Energy Surface. *J. Phys. Chem. A* **2010**, *114*, 4036–4044.
- (24) Li, A.; Yuan, S.; Dou, Y.; Wang, Y.; Wen, Z. Semiclassical Dynamic Simulation of Photon Induced Ring-Opening of Cyclohexadiene to Hexatriene. *Chem. Phys. Lett.* **2009**, *478*, 28–32.
- (25) Tapavicza, E.; Meyer, A. M.; Furche, F. Unravelling the Details of Vitamin D Photosynthesis by Non-Adiabatic Molecular Dynamics Simulations. *Phys. Chem. Chem. Phys.* **2011**, *13*, 20986–20998.
- (26) Kim, J.; Tao, H.; Martinez, T. J.; Bucksbaum, P. Ab Initio Multiple Spawning on Laser-Dressed States: A Study of 1,3-Cyclohexadiene Photoisomerization via Light-Induced Conical Intersections. *J. Phys. B: At. Mol. Opt. Phys.* **2015**, *48*, 164003.

- (27) Ohta, A.; Kobayashi, O.; Danielache, S. O.; Nanbu, S. Nonadiabatic ab Initio Molecular Dynamics of Photoisomerization Reaction between 1,3-Cyclohexadiene and 1,3,5-cis-Hexatriene. *Chem. Phys.* **2015**, *459*, 45–53.
- (28) Schalk, O.; Geng, T.; Thompson, T.; Baluyot, N.; Thomas, R. D.; Tapavicza, E.; Hansson, T. Cyclohexadiene Revisited: A Time-Resolved Photoelectron Spectroscopy and ab Initio Study. *J. Phys. Chem. A* **2016**, *120*, 2320–2329.
- (29) Lei, Y.; Wu, H.; Zheng, X.; Zhai, G.; Zhu, C. Photo-Induced 1,3-Cyclohexadiene Ring Opening Reaction: Ab Initio on-the-fly Nonadiabatic Molecular Dynamics Simulation. *J. Photochem. Photobiol. A* **2016**, *317*, 39–49.
- (30) Filatov, M.; Min, S. K.; Kim, K. S. Non-Adiabatic Dynamics of Ring Opening in Cyclohexa-1,3-diene Described by an Ensemble Density-Functional Theory Method. *Mol. Phys.* **2018**, DOI: 10.1080/00268976.2018.1519200.
- (31) Minitti, M. P.; Budarz, J. M.; Kirrander, A.; Robinson, J.; Lane, T. J.; Ratner, D.; Saita, K.; Northey, T.; Stankus, B.; Cofer-Shabica, V.; Hastings, J.; Weber, P. M. Toward Structural Femtosecond Chemical Dynamics: Imaging Chemistry in Space and Time. *Faraday Discuss.* **2014**, *171*, 81–91.
- (32) Minitti, M. P.; Budarz, J. M.; Kirrander, A.; Robinson, J. S.; Ratner, D.; Lane, T. J.; Zhu, D.; Glowonia, J. M.; Kozina, M.; Lemke, H. T.; Sikorski, M.; Feng, Y.; Nelson, S.; Saita, K.; Stankus, B.; Northey, T.; Hastings, J. B.; Weber, P. M. Imaging Molecular Motion: Femtosecond X-Ray Scattering of an Electrocyclic Chemical Reaction. *Phys. Rev. Lett.* **2015**, *114*, 255501.
- (33) Wolf, T. J. A.; Sanchez, D. M.; Yang, J.; Parrish, R. M.; Nunes, J. P. F.; Centurion, M.; Coffee, R.; Cryan, J. P.; Gühr, M.; Hegazy, K.; Kirrander, A.; Li, R. K.; Ruddock, J.; Shen, X.; Veccione, T.; Weathersby, S. P.; Weber, P. M.; Wilkin, K.;

- Yong, H.; Zheng, Q.; Wang, X. J.; Minitti, M. P.; Martínez, T. J. The Photochemical Ring-Opening of 1,3-Cyclohexadiene Imaged by Ultrafast Electron Diffraction. *Nat. Chem.* **2019**, DOI: 10.1038/s41557-019-0252-7.
- (34) Attar, A. R.; Bhattacharjee, A.; Pemmaraju, C. D.; Schnorr, K.; Closser, K. D.; Prendergast, D.; Leone, S. R. Femtosecond X-ray Spectroscopy of an Electrocyclic Ring-Opening Reaction. *Science* **2017**, *356*, 54–59.
- (35) Iikubo, R.; Sekikawa, T.; Harabuchi, Y.; Taketsugu, T. Structural Dynamics of Photochemical Reactions Probed by Time-Resolved Photoelectron Spectroscopy Using High Harmonic Pulses. *Faraday Discuss.* **2016**, *194*, 147–160.
- (36) Kaneshima, K.; Ninota, Y.; Sekikawa, T. Time-Resolved High-Harmonic Spectroscopy of Ultrafast Photoisomerization Dynamics. *Opt. Express* **2018**, *26*, 31039–31054.
- (37) Minnaard, N. G.; Havinga, E. Some Aspects of the Solution Photochemistry of 1,3-Cyclohexadiene, (Z)- and (E)-1,3,5-Hexatriene. *Recl. Trav. Chim. Pays-Bas* **1973**, *92*, 1315–1320.
- (38) Ruan, C.-Y.; Lobastov, V. A.; Srinivasan, R.; Goodson, B. M.; Ihee, H.; Zewail, A. H. Ultrafast Diffraction and Structural Dynamics: The Nature of Complex Molecules Far from Equilibrium. *Proc. Natl. Acad. Sci.* **2001**, *98*, 7117–7122.
- (39) Dudek, R. C.; Weber, P. M. Ultrafast Diffraction Imaging of the Electrocyclic Ring-Opening Reaction of 1,3-Cyclohexadiene. *J. Phys. Chem. A* **2001**, *105*, 4167–4171.
- (40) White, J. L.; Kim, J.; Petrović, V. S.; Bucksbaum, P. H. Ultrafast Ring Opening in 1,3-Cyclohexadiene Investigated by Simplex-Based Spectral Unmixing. *J. Chem. Phys.* **2012**, *136*, 054303.
- (41) Kotur, M.; Weinacht, T.; Pearson, B. J.; Matsika, S. Closed-Loop Learning Control of

- Isomerization Using Shaped Ultrafast Laser Pulses in the Deep Ultraviolet. *J. Chem. Phys.* **2009**, *130*, 134311.
- (42) Tian, T.; Xu, T.; Kirk, S. R.; Filatov, M.; Jenkins, S. Next-Generation Quantum Theory of Atoms in Molecules for the Ground and Excited State of the Ring-Opening of Cyclohexadiene. *Int. J. Quant. Chem.* **2018**, DOI: 10.1002/qua.25862.
- (43) Santolini, V.; Malhado, J. P.; Robb, M. A.; Garavelli, M.; Bearpark, M. J. Photochemical Reaction Paths of cis-Dienes Studied with RASSCF: The Changing Balance Between Ionic and Covalent Excited States. *Mol. Phys.* **2015**, *113*, 1978–1990.
- (44) Kim, J.; Tao, H.; White, J. L.; Petrović, V. S.; Martinez, T. J.; Bucksbaum, P. H. Control of 1,3-Cyclohexadiene Photoisomerization Using Light-Induced Conical Intersections. *J. Phys. Chem. A* **2012**, *116*, 2758–2763.
- (45) Tao, H. First Principles Molecular Dynamics and Control of Photochemical Reactions. Ph.D. thesis, Stanford University, 2011.
- (46) Park, J. W.; Shiozaki, T. Analytical Derivative Coupling for Multistate CASPT2 Theory. *J. Chem. Theory Comput.* **2017**, *13*, 2561–2570.
- (47) Park, J. W.; Shiozaki, T. On-the-Fly CASPT2 Surface-Hopping Dynamics. *J. Chem. Theory Comput.* **2017**, *13*, 3676–3683.
- (48) Shiozaki, Toru, BAGEL, Brilliantly Advanced General Electronic-structure Library. <http://www.nubakery.org>, under the GNU General Public License.
- (49) Shiozaki, T. BAGEL : Brilliantly Advanced General Electronic-structure Library. *WIREs Comput. Mol. Sci.* **2018**, *8*, e1331, DOI: 10.1002/wcms.1331.
- (50) Roos, B. O.; Andersson, K. Multiconfigurational Perturbation Theory with Level Shift - the Cr<sub>2</sub> Potential Revisited. *Chem. Phys. Lett.* **1995**, *245*, 215–223.

- (51) Dunning Jr., T. H. Gaussian Basis Sets for Use in Correlated Molecular Calculations. I. The Atoms Boron Through Neon and Hydrogen. *J. Chem. Phys.* **1989**, *90*, 1007–1023.
- (52) Bearpark, M. J.; Robb, M. A.; Schlegel, H. B. A Direct Method for the Location of the Lowest Energy Point on a Potential Surface Crossing. *Chem. Phys. Lett.* **1994**, *223*, 269 – 274.
- (53) Barbatti, M.; Ruckebauer, M.; Plasser, F.; Pittner, J.; Granucci, G.; Persico, M.; Lischka, H. Newton-X: A Surface-Hopping Program for Nonadiabatic Molecular Dynamics. *WIREs: Comp. Mol. Sci.* **2014**, *4*, 26–33.
- (54) Barbatti, M. and Granucci, G. and Ruckebauer, M. and Plasser, F. and Crespo-Otero, R. and Pittner, J. and Persico, M. and Lischka, H., NEWTON-X: A Package for Newtonian Dynamics Close to the Crossing Seam. 2016; [www.newtonx.org](http://www.newtonx.org), Version 2.
- (55) Crespo-Otero, R.; Barbatti, M. Spectrum Simulation and Decomposition with Nuclear Ensemble: Formal Derivation and Application to Benzene, Furan and 2-Phenylfuran. *Theor. Chem. Acc.* **2012**, *131*, 1237.
- (56) Granucci, G.; Persico, M. Critical Appraisal of the Fewest Switches Algorithm for Surface Hopping. *J. Chem. Phys.* **2007**, *126*, 134114.
- (57) Tully, J. C. Molecular Dynamics with Electronic Transitions. *J. Chem. Phys.* **1990**, *93*, 1061–1071.
- (58) Nangia, S.; Jasper, A. W.; Miller III, T. F.; Truhlar, D. G. Army Ants Algorithm for Rare Event Sampling of Delocalized Nonadiabatic Transitions by Trajectory Surface Hopping and the Estimation of Sampling Errors by the Bootstrap Method. *J. Chem. Phys.* **2004**, *120*, 3586–3597.
- (59) Yue, L.; Yu, L.; Xu, C.; Lei, Y.; Liu, Y.; Zhu, C. Benchmark Performance of Global Switching versus Local Switching for Trajectory Surface Hopping Molecular Dynamics

Simulation: Cis  $\leftrightarrow$  Trans Azobenzene Photoisomerization. *Chem. Phys. Chem.* **2017**, *18*, 1274–1287.

- (60) Tudorovskaya, M.; Minns, R. S.; Kirrander, A. Effect of Probe Energy and Competing Pathways on Time-Resolved Photoelectron Spectroscopy: The Ring-Opening Reaction of 1,3-Cyclohexadiene. *Phys. Chem. Chem. Phys.* **2018**, *20*, 17714–17726.

# Graphical TOC Entry

